# *foxl3*, a sexual switch in germ cells, initiates two independent molecular pathways for commitment to oogenesis in medaka

Mariko Kikuchi[a], Toshiya Nishimura[a,1], Satoshi Ishishita[b], Yoichi Matsuda[b,c], and Minoru Tanaka[a,2]

[a]Division of Biological Science, Graduate School of Science, Nagoya University, 464-8602 Nagoya, Japan; [b]Avian Bioscience Research Center, Graduate School of Bioagricultural Sciences, Nagoya University, 464-8601 Nagoya, Japan; and [c]Department of Animal Sciences, Graduate School of Bioagricultural Sciences, Nagoya University, 464-8601 Nagoya, Japan

Edited by John J. Eppig, The Jackson Laboratory, Bar Harbor, ME, and approved April 8, 2020 (received for review October 23, 2019)

**Germ cells have the ability to differentiate into eggs and sperm and must determine their sexual fate. In vertebrates, the mechanism of commitment to oogenesis following the sexual fate decision in germ cells remains unknown. *Forkhead-box protein L3* (*foxl3*) is a switch gene involved in the germline sexual fate decision in the teleost fish medaka (*Oryzias latipes*). Here, we show that *foxl3* organizes two independent pathways of oogenesis regulated by *REC8 meiotic recombination protein a* (*rec8a*), a cohesin component, and *F-box protein* (FBP) *47* (*fbxo47*), a subunit of E3 ubiquitin ligase. In mutants of either gene, germ cells failed to undergo oogenesis but developed normally into sperm in testes. Disruption of *rec8a* resulted in arrest at a meiotic pachytenelike stage specifically in females, revealing a sexual difference in meiotic progression. Analyses of *fbxo47* mutants showed that this gene regulates transcription factors that facilitate folliculogenesis: *LIM homeobox 8* (*lhx8b*), *factor in the germline* α (*figla*), and *newborn ovary homeobox* (*nobox*). Interestingly, we found that the *fbxo47* pathway ensures that germ cells do not deviate from an oogenic pathway until they reach diplotene stage. The mutant phenotypes together with the timing of their expression imply that germline feminization is established during early meiotic prophase I.**

germline sex determination | *foxl3* | *rec8a* | *fbxo47* | oogenesis commitment

Germ cells, which have the potential to differentiate into eggs and sperm, must determine their sexual fate. In the teleost fish medaka (*Oryzias latipes*), the onset of the germline sexual fate decision is triggered by *foxl3* (*forkhead box protein L3*) (1). During medaka gonadal development, *foxl3* expression is maintained only in female germ cells, and the loss-of-function mutant of *foxl3* results in production of functional sperm in the ovary, indicating that *foxl3* is required for suppression of spermatogenesis in female germ cells (1). However, the specific role of *foxl3* in germline feminization (process of commitment to oogenesis) has not been clarified.

To elucidate the molecular pathways organized by *foxl3*, we previously identified *rec8a* (*REC8 meiotic recombination protein a*) and *fbxo47* (*F-box protein 47*) as direct targets of FOXL3 (2). *rec8a* and *fbxo47* transcripts are detected in mitotic germ cells expressing *foxl3* in wild-type ovaries but not in *foxl3*$^{-/-}$ ovaries and are indicated to act downstream of *foxl3* during germline sex determination (2). *rec8a* is one of two *Rec8* orthologs resulting from the teleost-specific whole-genome duplication (3). REC8 is a meiosis-specific kleisin subunit of the cohesin complex, which plays crucial roles in various meiosis-associated chromosomal events, including chromosomal axis formation and homolog association (4). *Rec8*-null mutant mice of both sexes are sterile and fail to complete meiotic prophase I (5, 6). On the other hand, the F-box domain-containing protein FBXO47 has been implicated to act as a subunit of Skp1-cullin1-FBP (SCF)-type E3 ubiquitin ligases (7). Notably, germ cells in the *fbxo47* mutant exhibit defects in meiotic recombination in both mice and *Caenorhabditis elegans* (8–10). To date, however, neither protein has been implicated in germline feminization.

During oogenesis in mice, several transcription factors facilitate folliculogenesis: *lhx8* (*LIM homeobox 8*) and *figla* (*factor in the germline alpha*) regulate differentiation of primordial follicles (11–14), and *nobox* (*newborn ovary homeobox*), which acts downstream of *Lhx8*, is indispensable for the formation of secondary follicles (12, 15). It remains unknown how these transcription factors cooperate after sexually indifferent germ cells commit to oogenesis.

Here, we show that *foxl3* orchestrates two independent pathways for oogenesis: one leading to meiosis by *rec8a* and the other to follicle development by *fbxo47*. In addition, we show that the *fbxo47*-downstream pathway ensures that germ cells do not deviate from the oogenesis pathway during early meiotic prophase I; otherwise, the sexual fate of the germ cells would change to spermatogenesis. Thus, we propose that the diplotene stage of meiotic prophase I is the point of no return for establishing germline feminization.

## Results

***rec8a* Is Required for Female Meiotic Progression.** To investigate the function of *rec8a* in germline feminization, we generated *rec8a*

### Significance

In teleost fish, unlike mammals, retinoic acid (RA) does not exert a conspicuous feminization effect of germ cells. Instead, in the teleost fish medaka, *foxl3* serves as a germ cell-autonomous factor acting at the very beginning of the sexual fate decision. This study shows that *foxl3* initiates oogenesis through two genetically independent pathways, meiosis and follicular development. One pathway, involving *rec8a*, drives female-specific regulation of meiosis. The other, involving *fbxo47*, both directs follicular development and suppresses spermatogenesis commitment. The involvement of two evolutionarily conserved factors in oogenesis suggests the existence of an RA-independent pathway that promotes oogenesis, common in vertebrates. In addition, our findings reveal the timing of the establishment of germ cell feminization.

Author contributions: M.K. and M.T. designed research; M.K., T.N., and S.I. performed research; T.N. contributed new reagents/analytic tools; M.K., S.I., Y.M., and M.T. analyzed data; and M.K. and M.T. wrote the paper.

The authors declare no competing interest.

This article is a PNAS Direct Submission.



[1]Present address: Division of Marine Life Science, Graduate School of Fisheries Sciences, Hokkaido University, 041-8611 Hakodate, Japan.

[2]To whom correspondence may be addressed. Email: mtanaka@bio.nagoya-u.ac.jp.

This article contains supporting information online at https://www.pnas.org/lookup/suppl/doi:10.1073/pnas.1918556117/-/DCSupplemental.

First published May 14, 2020.

mutants by CRISPR/Cas9 (*SI Appendix*, Fig. S1). *rec8a*$^{-/-}$ XY males developed normal testes with mature sperm (*SI Appendix*, Fig. S2 *A* and *B*). Although the hatching rate of eggs fertilized with *rec8a*$^{-/-}$ XY sperm was slightly lower than that of eggs with wild-type sperm, *rec8a*$^{-/-}$ XY sperm were fertile (*SI Appendix*, Fig. S2 *C* and *D*). On the other hand, *rec8a*$^{-/-}$ XX females were sterile, and all of the mutant ovaries lacked follicles (Fig. 1 *A* and *B*). Because we could not find germ cells at the diplotene stage in the mutant ovaries, meiosis was likely arrested before the diplotene stage (Fig. 1 *A* and *B*, *Insets*).

We next examined the synaptonemal complex (SC) formation in *rec8a*$^{-/-}$ ovaries. In the control (*rec8a*$^{+/-}$) ovaries, synapsis marker SYCP1 (a central element of SC) localized between homologous chromosomes of zygotene to pachytene oocytes, and these signals disappeared in diplotene oocytes (Fig. 1 *C*–*E*). In *rec8a*$^{-/-}$ ovaries, although SYCP1 localized normally to the forming SC axes of zygotene chromosomes, the signal became punctate at a pachytenelike stage (Fig. 1 *F*–*H*). These results suggest that SC axes prematurely disassembled in the *rec8a*$^{-/-}$ oocytes and that *rec8a* is required for the stability of the SC axis during the pachytene stage.

To explore the possibility that abnormal oocytes were eliminated by apoptosis, we immunostained for activated caspase-3 (cleaved caspase-3 [CC-3]) in wild-type and *rec8a*$^{-/-}$ ovaries. We first measured the length of the oocyte long axis (diameter) at zygotene, pachytene, and diplotene stages in wild-type ovaries and found that the diameter of pachytene oocytes ranged from 15 to 25 μm (*SI Appendix*, Table S1). Immunostaining of *rec8a*$^{-/-}$ ovaries revealed that most CC-3-positive germ cells with fragmented DNA had a pachytenelike diameter (Fig. 1 *I* and *J* and *SI Appendix*, Table S2). These CC-3-positive pachytenelike oocytes (long axis: 15–25 μm) accumulated at higher levels in *rec8a*$^{-/-}$ than in wild-type ovaries (Fig. 1*K*). This observation, combined with the mutant phenotype, suggests that aberrant *rec8a*$^{-/-}$oocytes were removed by apoptosis.

***fbxo47* Is Involved in Suppression of Spermatogenesis in Female Germ Cells.** To examine the function of *fbxo47*, we developed a germline-targeted mutant of this gene (*SI Appendix*, Fig. S3). *fbxo47*-mutant XX ovaries exhibited a defect in folliculogenesis (Fig. 2*A*), whereas mutant XY testes did not have any remarkable phenotype (Fig. 2*B*). In the mutant ovaries, we observed germ cells with abnormally condensed chromosomes (Fig. 2 *A*, *Inset* arrowheads). Whole-mount immunostaining, combined with 3D reconstruction of DAPI signals, revealed that *fbxo47*-mutant germ cells contained U-shaped chromosomes (*SI Appendix*, Fig. S4 *A* and *B*). The U-shaped chromosomes were positive for phosphorylated histone H3, which is present in mitotic germ cells in wild-type ovaries (*SI Appendix*, Fig. S4 *C*–*E*). Chromosome spreads revealed that the chromosomes in mitotically dividing *fbxo47*-mutant nuclei ($2n$ = 48) were highly condensed (*SI Appendix*, Fig. S4*G*), consistent with the images in *SI Appendix*, Fig. S4 *B* and *B′*. By contrast, control chromosomes at the same stage were well extended (*SI Appendix*, Fig. S4*F*). These results suggest that cell division was impaired or delayed at metaphase in *fbxo47*-mutant ovaries and that *fbxo47* is associated with regulation of mitotic chromosomal structure.

Surprisingly, *fbxo47*-mutant ovaries developed spermlike cells with small condensed nuclei in the expanded germinal epithelium (Fig. 2 *A*, *Inset* arrows). To examine the process of gametogenesis in detail, we observed the chromosomal morphology of meiotic germ cells in wild-type ovaries, wild-type testes, and *fbxo47*-mutant ovaries (Fig. 2*C*). In wild-type ovaries and testes, chromosomes gradually condensed and synapsed by the pachytene stage of meiotic prophase I. After the pachytene stage, gametogenesis proceeds differently between males and females: Oogenesis arrests at the diplotene stage (Fig. 2 *C*, *Top*), whereas, in spermatogenesis, the second meiotic division is completed, followed by spermiogenesis (Fig. 2 *C*, *Middle*). Intriguingly, the chromosomal morphology in some population of germ cells in *fbxo47* mutants was similar to that observed in wild-type spermatogenesis (Fig. 2 *C*, *Bottom*, and *SI Appendix*, Fig. S4*H*).

To test the hypothesis that *fbxo47*-mutant germ cells committed to spermatogenesis, we examined the expression of *shippo1b*, a spermatocyte and spermatid marker, by in situ hybridization. The *shippo1b* signal was detected in both the control wild-type XY testes and the *fbxo47*-mutant XX ovaries (Fig. 2 *D* and *E*). Interestingly, *shippo1b* was already expressed in *fbxo47*$^{-/-}$ XX gonads at 15 days posthatching (dph), consistent with the time when spermatogenesis initiated in the *foxl3*$^{-/-}$ XX gonads (1) (Fig. 2 *F* and *G* and *SI Appendix*, Fig. S5).

To further analyze the function of *fbxo47*, we introduced a bacterial artificial chromosome (BAC) containing the *fbxo47* allele with enhanced green fluorescent protein (EGFP) into *foxl3* mutants (*SI Appendix*, Fig. S6 and Table S3). None of the EGFP-expressing germ cells in *foxl3*$^{-/-}$ XX gonads ($n$ = 5) exhibited spermatogenic progression (Fig. 2 *H* and *I*). Collectively, these data strongly suggest that *fbxo47* is a downstream factor of *foxl3* that is essential for suppressing spermatogenesis.

**Two Pathways Downstream of *foxl3* Contribute to Germline Feminization.** As described above, two *foxl3*-downstream genes *rec8a* and *fbxo47* are female-specific regulators of meiosis progression and suppression of spermatogenesis, respectively. To examine the relationship between these two genes and the transcription factors involved in early folliculogenesis, we generated medaka mutants of *lhx8b*, *figla*, and *nobox*, and analyzed the phenotypes with regard to the functions of *rec8a* and *fbxo47*.

One of the two medaka *Lhx8* orthologs *lhx8b* was up-regulated downstream of *foxl3* as determined by RNA sequencing (2). The *lhx8b* mutant exhibited female-specific defects in gametogenesis: It developed typical ovarian structures that contained no follicles (Fig. 3*A* and *SI Appendix*, Fig. S7). Instead, the *lhx8b*$^{-/-}$ ovaries contained spermatocyte- and spermlike cells (Fig. 3*A*, arrows). In addition, *shippo1b* was expressed in the *lhx8b*$^{-/-}$ ovaries (Fig. 3*B*), suggesting that germ cells undergo spermatogenesis.

*figla* expression in medaka is first detected in germ cells at early meiotic prophase I (16). In medaka *figla*$^{-/-}$ ovaries (16), folliculogenesis is disrupted as in mouse *Figla*-knockout (KO) ovaries (14). Careful observations of medaka *figla*$^{-/-}$ ovaries revealed the presence of spermlike cells with small condensed nuclei within the expanded germinal epithelium (Fig. 3*C*, arrows). In addition, *shippo1b* was expressed in the *figla*$^{-/-}$ ovaries (Fig. 3*D*). These results suggest that *figla*$^{-/-}$ germ cells, such as *fbxo47*$^{-/-}$ and *lhx8b*$^{-/-}$ germ cells, committed to spermatogenesis.

Next, we examined the *nobox* mutant phenotype (*SI Appendix*, Fig. S8 *A*–*C*). The *nobox*$^{-/-}$ mutants exhibited female-specific infertility and developed small ovaries devoid of large follicles (Fig. 3*E*). Histological analysis revealed that follicles were normally formed (Fig. 3 *F* and *G*) but their growth was arrested at the stage of 300 μm-diameter oocyte in *nobox*$^{-/-}$ ovaries (*SI Appendix*, Fig. S8*D*). These data suggest that, in medaka, as in mammals, *nobox* is required for follicle growth.

Finally, we conducted molecular epistasis analysis for *rec8a*, *fbxo47*, *lhx8b*, *figla*, and *nobox* using these mutants. In wild-type ovaries, *rec8a* expressed in mitotic germ cells, *fbxo47* expressed in mitotic and early meiotic (leptotene to zygotene) germ cells, *lhx8b* expressed from leptotene to mainly zygotene oocytes, and *figla* and *nobox* expressed from zygotene to mainly diplotene oocytes (Fig. 4 *A*, *E*, *I*, *M*, and *Q*). In *rec8a*$^{-/-}$ ovaries, all genes examined were expressed (Fig. 4 *F*, *J*, *N*, and *R*). On the other hand, in *fbxo47*$^{-/-}$ ovaries, expression of *lhx8b*, *figla*, and *nobox* was not detected, whereas *rec8a* was expressed (Fig. 4 *B*, *K*, *O*, and *S*). In *lhx8b*$^{-/-}$ ovaries, expression of *figla* and *nobox* was not observed, but *rec8a* and *fbxo47* were expressed (Fig. 4 *C*, *G*, *P*, and *T*). In *figla*$^{-/-}$ ovaries, *nobox* expression was not observed, but the other genes were expressed (Fig. 4 *D*, *H*, *L*, and *U*).

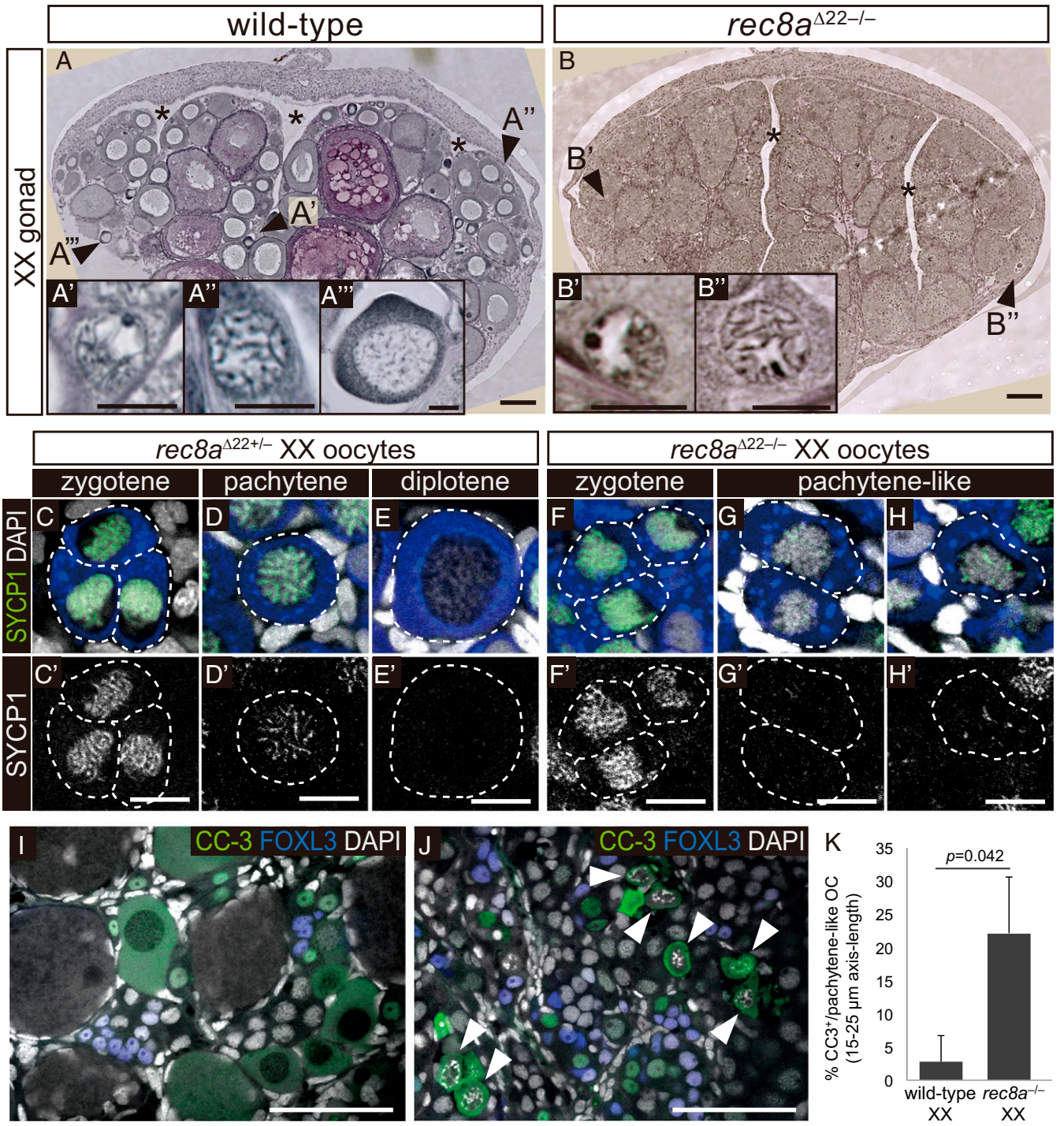


**Fig. 1.** *rec8a* is required for female meiosis. (*A* and *B*) Periodic acid–Schiff (PAS) staining of 2.5-mo-old wild-type (*A*, $n = 3$) and *rec8a*$^{\Delta 22-/-}$ (*B*, $n = 2$) XX gonads. Magnified images of zygotene (*A′* and *B′*), pachytene (*A″* and *B″*), and diplotene (*A‴*) oocytes, indicated by arrowheads, are shown in the *Insets*. Bouquet chromosomal structure and paired bivalents were observed in zygotene and pachytene oocytes, respectively. Asterisks in *A* and *B* indicate the ovarian cavity, a typical ovarian structure of medaka. (Scale bars: 100 μm [*A* and *B*], 10 μm (*A′*, *A″* *A‴*, *B′*, and *B″*). (*C–H*) Immunohistochemistry (IHC) of 10-dph *rec8a*$^{\Delta 22+/-}$ (*C–E*, $n = 5$) and *rec8a*$^{\Delta 22-/-}$ (*F–H*, $n = 4$) XX ovaries. In the *Top*, samples were stained for a synapsis marker SYCP1 (green) and a germ cell marker OLVAS (blue) with DAPI staining (gray). Gray scale images of SYCP1 signals are shown in the *Bottom*. Germ cells indicated by dotted lines represent zygotene (*C* and *F*), pachytene (*D*), diplotene (*E*), and pachytenelike stages (*G* and *H*) characterized by cellular sizes and chromosomal structures. (Scale bar: 10 μm.) (*I* and *J*) Immunostaining of XX adult ovaries of wild-type (*I*, $n = 3$) and *rec8a*$^{\Delta 8-/-}$ fish (*J*, $n = 3$) for cleaved CC-3 (green) and a female mitotic germ cell marker FOXL3 (blue) with DAPI staining (gray). Arrowheads in *J* indicate CC-3-positive germ cells with DAPI-dense DNA fragments. (Scale bar: 50 μm.) (*K*) Percentage of CC-3-positive germ cells in pachytenelike oocytes (length of long axis: 15–25 μm, *SI Appendix*, Table S1) in wild-type and *rec8a*$^{-/-}$ XX ovaries. Values are means ± SD from three ovaries. *P* value was calculated by two-tailed Student's *t* test. Exact values are shown in *SI Appendix*, Table S2.

To summarize, there are, at least, two genetically independent pathways downstream of *foxl3* (Fig. 5): the *rec8a*-dependent pathway, which regulates progression of meiosis in female medaka, and the *fbxo47*-dependent pathway, which suppresses germ cell commitment to spermatogenesis and promotes folliculogenesis. Interestingly, ovaries harboring mutations in *fbxo47*, *lhx8b*, or *figla* developed spermatocytes, whereas *nobox*-mutant ovaries did not. The mutant phenotypes along with the timing of gene expression in germ cells suggest that spermatogenesis is continuously repressed until the diplotene stage in order to establish germline feminization.

## Discussion

In general, vertebrate meiosis initiates much earlier in the ovary than in the testis. Oogenesis with meiosis occurs during embryogenesis in many vertebrates, while meiosis in the testis starts after the onset of puberty. Accordingly, entry into meiosis is considered a hallmark of feminization of germ cells. In mammals,

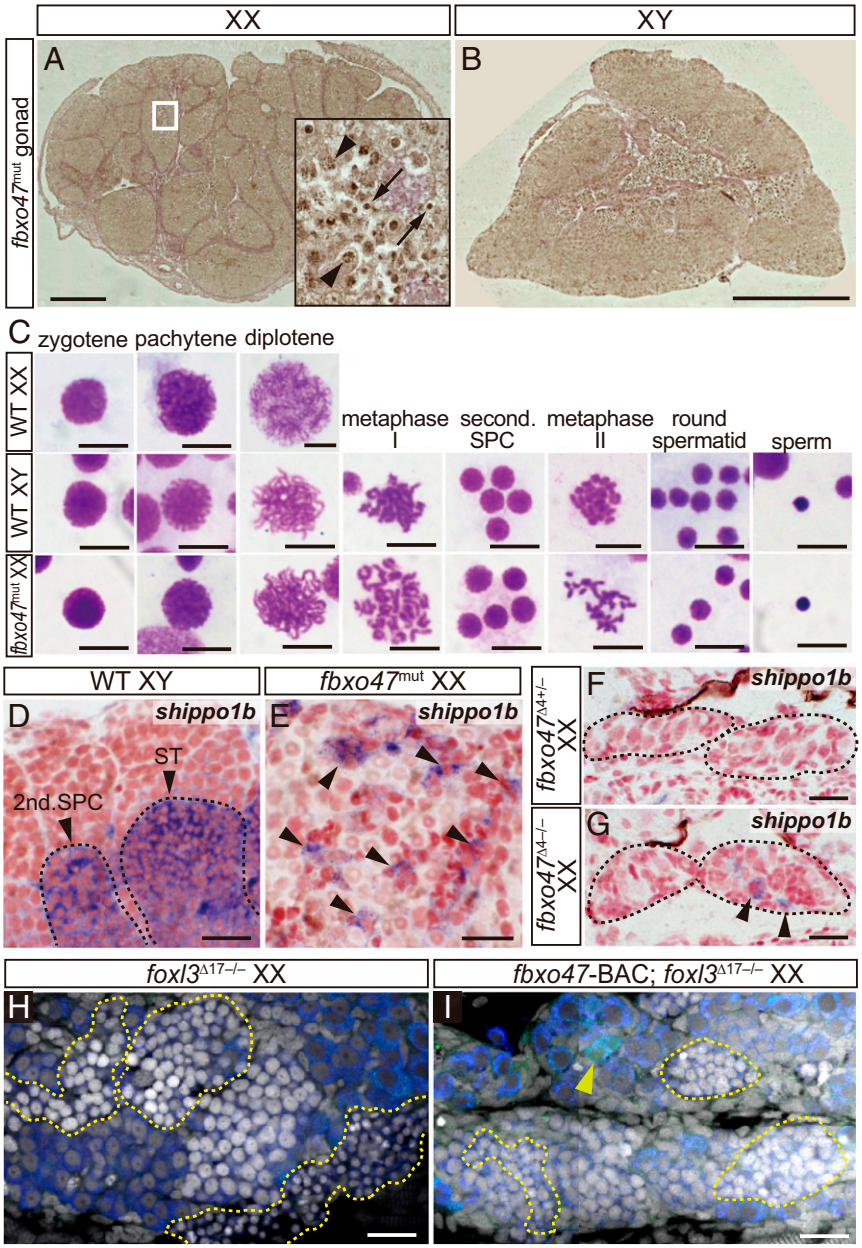


**Fig. 2.** *fbxo47* is involved in suppression of spermatogenesis in female germ cells. (*A* and *B*) PAS staining of 4-mo-old *fbxo47*-mutant XX (*A*, $n = 2/3$) and XY (*B*, $n = 2$) gonads. *Inset* in *A* is a magnified image of the region indicated by the white square. Arrowheads and arrows indicate germ cells with abnormally condensed chromosomes and spermlike cells, respectively. (Scale bars: 200 μm.) (*C*) Giemsa staining of meiotic chromosomes of wild-type XX (*Top*), wild-type XY (*Middle*), and *fbxo47*-mutant XX (*Bottom*) germ cells. The meiotic stage is shown above each panel. spermatocyte (SPC). (Scale bar: 10 μm.) (*D*–*G*) In situ hybridization for *shippo1b*, a marker of secondary SPCs (second. SPC) and spermatids (ST), using wild-type testes (*D*, $n = 3$), *fbxo47*-mutant ovaries (*E*, $n = 3$), $fbxo47^{\Delta 4+/-}$ 10-dph XX gonads (*F*, $n = 2$), and $fbxo47^{\Delta 4-/-}$ 10-dph XX gonads (*G*, $n = 4$). Arrowheads indicate *shippo1b*-expressing cells (blue). Germ cell cysts (*D*) or 10-dph gonads (*F* and *G*) are outlined by dotted lines. (Scale bar: 20 μm.) (*H* and *I*) Immunostaining of 10-dph $foxl3^{\Delta 17-/-}$ XX gonads (*H*, $n = 6$) and *fbxo47*-induced $foxl3^{\Delta 17-/-}$ XX gonads (*I*, $n = 5$) for OLVAS (red), EGFP (green), and DAPI (gray). Yellow dotted lines indicate secondary SPCs and STs. All EGFP+ germ cells observed in *fbxo47*-induced gonads were mitotic (arrowhead in *I*), suggesting that ectopic *fbxo47* expression suppressed progression of spermatogenesis in $foxl3^{\Delta 17-/-}$ XX gonads. In *I*, two images taken from the anterior and posterior regions of the same gonad were merged to produce a single entire image. (Scale bar: 20 μm.)

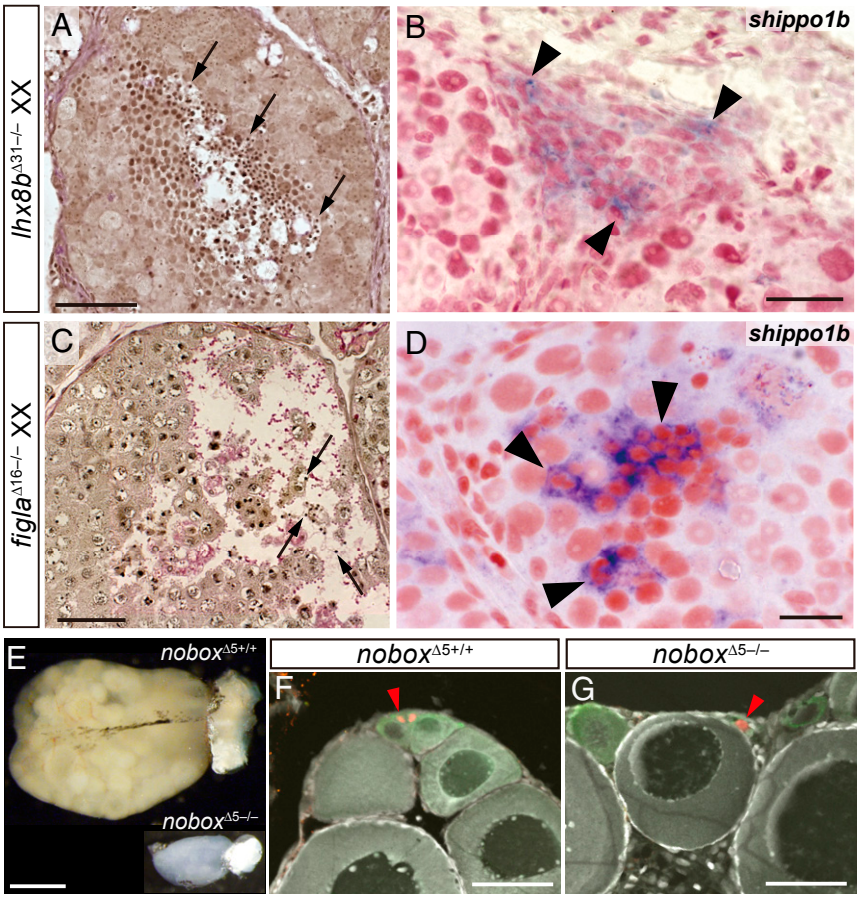


**Fig. 3.** *lhx8b* and *figla* but not *nobox* are related to suppression of spermatogenesis. (*A*) PAS staining of *lhx8b*$^{\Delta 31-/-}$ XX gonads. Arrows indicate spermlike cells. (Scale bar: 50 μm.) $n = 4$. (*B*) *shippo1b* expression in *lhx8b*$^{\Delta 31-/-}$ XX ovaries. Arrowheads indicate *shippo1b*-expressing germ cells. Bar: 20 μm. $n = 3$. (*C*) PAS staining of *figla*$^{\Delta 16-/-}$ XX gonads. Arrows indicate spermlike cells. (Scale bar: 50 μm.) $n = 3$. (*D*) *shippo1b* expression in *figla*$^{\Delta 16-/-}$ XX ovaries. Arrowheads indicate *shippo1b*-expressing germ cells. (Scale bar: 20 μm.) $n = 5$. (*E*) Gonadal morphology of 4-mo-old *nobox*$^{\Delta 5+/+}$ (*Top*) and *nobox*$^{\Delta 5-/-}$ (*Bottom*) XX ovaries. (Scale bar: 1 mm.) (*F* and *G*) IHC of *nobox*$^{\Delta 5+/+}$ (*F*, $n = 4$) and *nobox*$^{\Delta 5-/-}$ (*G*, $n = 2$) XX ovaries for OLVAS (green), and FOXL3 (red) with DAPI staining (gray). (Scale bar: 50 μm.)

bone morphogenetic protein and retinoic acid (RA) signaling induce female-type differentiation (oogenesis) and meiosis, respectively (17–22). By contrast, in medaka, it appears that RA signaling does not play a critical role in meiosis initiation during the sex determination period (23). Furthermore, a RA-responsive gene, *stimulated by retinoic acid gene 8*, has been lost from most teleost genomes (24).

Identification of *foxl3* as a sexual switch in medaka reveals that the process of sex determination in germ cells begins much earlier than a series of meiotic events. In this study, we successfully linked the regulatory mechanisms of oogenesis with germline sex determination where *rec8a* and *fbxo47* are critical effectors that initiate germline feminization downstream of the germline sexual switch *foxl3*. The pathways controlled by these two genes are independent genetically (Fig. 5).

Interestingly, the phenotype of the *rec8a* mutant indicates that *rec8a* is required for progression of oogenesis but not spermatogenesis. This raises the possibility that meiotic progression is regulated differently between the sexes. Consistent with this, sexual dimorphisms in meiosis, such as the number of crossovers per nucleus, axis length of meiotic chromosomes, and recombination rate, have been reported in several animals (25–29). Although the molecular mechanisms responsible for generating such sexual dimorphisms have not been elucidated, functional investigation of *rec8a* may provide insight into the role of sexual dimorphisms in meiosis.

*fbxo47*-mutant ovaries exhibited two main phenotypes: abnormal morphology of chromosomes and commitment to spermatogenesis. In *C. elegans*, disruption of the *fbxo47* homolog and *progression of meiosis 1* causes defects in meiotic processes, such as homologous pairing and synapsis (9). In rice (*Oryza sativa*), the F-box proteins MEIOTIC F-BOX and ZYGOTENE1 are involved in double-strand break repair and formation of bouquet structure of zygotene chromosomes, respectively (30, 31). These data may collectively imply that the functions of F-box proteins regulate germ cell chromosomal structure not only in mitosis, but also in meiosis in sexually reproductive organisms.

The precocious spermatogenesis in *fbxo47*$^{-/-}$ ovaries partially phenocopied that observed in *foxl3*$^{-/-}$ ovaries (1). This demonstrates that *fbxo47* is involved in suppression of spermatogenesis downstream of *foxl3*. Supporting this, germ cells artificially inducing *fbxo47* in the *foxl3*$^{-/-}$ female (XX) did not show any progress of spermatogenesis. In addition, two *fbxo47*-downstream genes *lhx8b* and *figla*, which are expressed in early meiotic prophase I, are also involved in the process of germline feminization as we found that disruption of either gene induced spermatogenesis in ovaries. By contrast, germ cells in *nobox*$^{-/-}$ ovaries did not develop spermatogenic cells. These results suggest that germline sex is fixed before the follicles start to grow at diplotene stage of meiosis I. Thus, although *foxl3* turns on the switch of the germline sex determination pathway during the mitotic phase (1), our results suggest that the sex of the

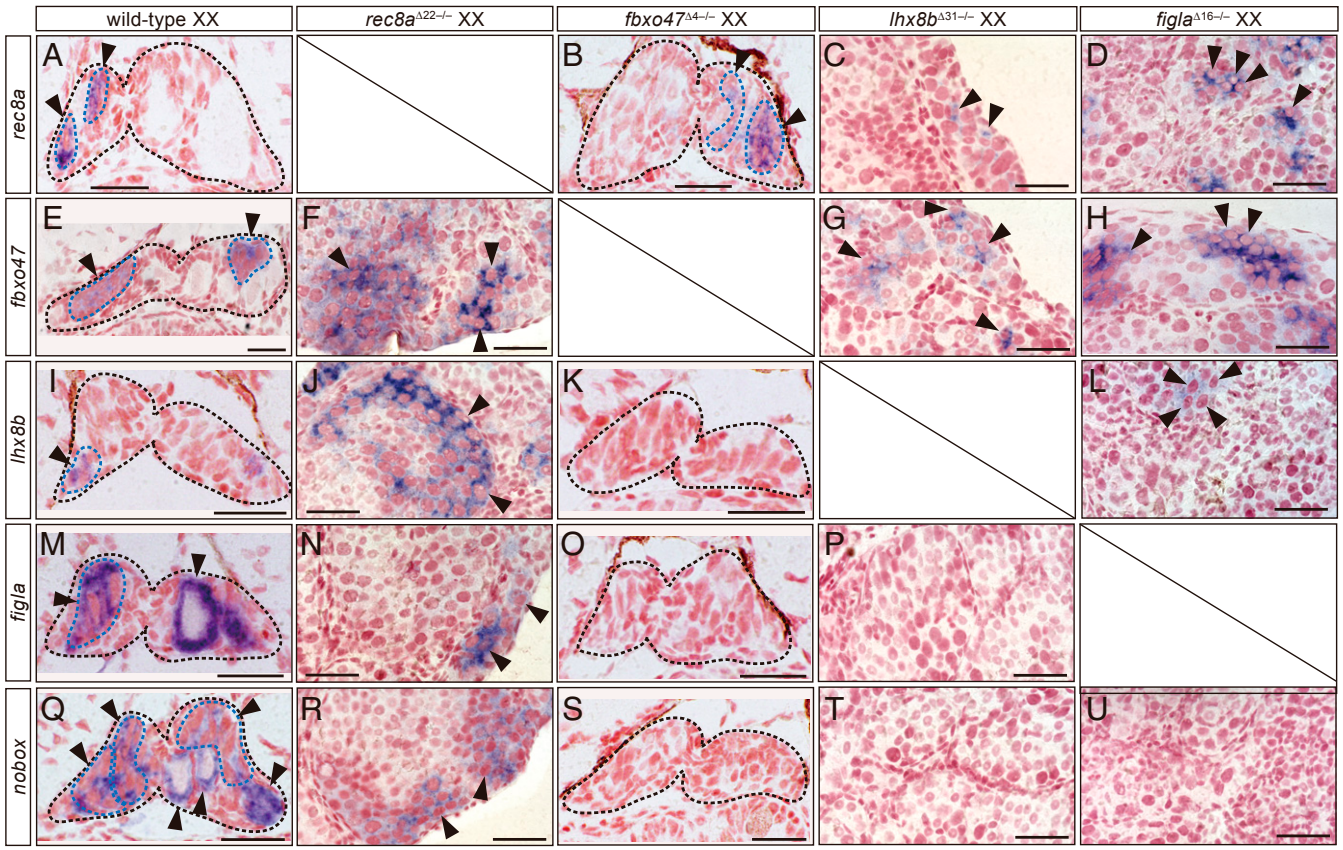


**Fig. 4.** Two pathways downstream of *foxl3* contribute to germline feminization. In situ hybridization for *rec8a* (*A–D*), *fbxo47* (*E–H*), *lhx8b* (*I–L*), *figla* (*M–P*), and *nobox* (*Q–U*) using wild-type XX 10 dph (*A*, *E*, *I*, *M*, and *Q*, $n = 3$), *rec8a*$^{\Delta 22-/-}$ XX (*F*, *J*, *N*, and *R*, $n = 3$), *fbxo4*$^{7\Delta 4-/-}$ XX 10 dph (*B*, *K*, *O*, and *S*, $n = 3$), *lhx8b*$^{\Delta 31-/-}$ XX (*C*, *G*, *P*, and *T*, $n = 3$), and *figla*$^{\Delta 16-/-}$ XX gonads (*D*, *H*, *L*, and *U*, $n = 3$). Arrowheads indicate signal-positive germ cells (blue). The 10-dph gonads of wild type and *fbxo47*$^{\Delta 4-/-}$ are outlined by black dotted lines. Blue dotted lines indicate germ cell cysts in 10-dph gonads. (Scale bar: 30 μm.)

germline is established during early meiotic prophase I. We propose that the diplotene stage, just before the follicles form but have not yet grown, is the point of no return for germline sex determination (Fig. 5).

Lastly, it may be worth noting that *atp1a3a* is up-regulated in female germ cells independently of *foxl3* (2). In addition to the two pathways revealed in this study, another molecular pathway might function during the course of germline feminization (Fig. 5).

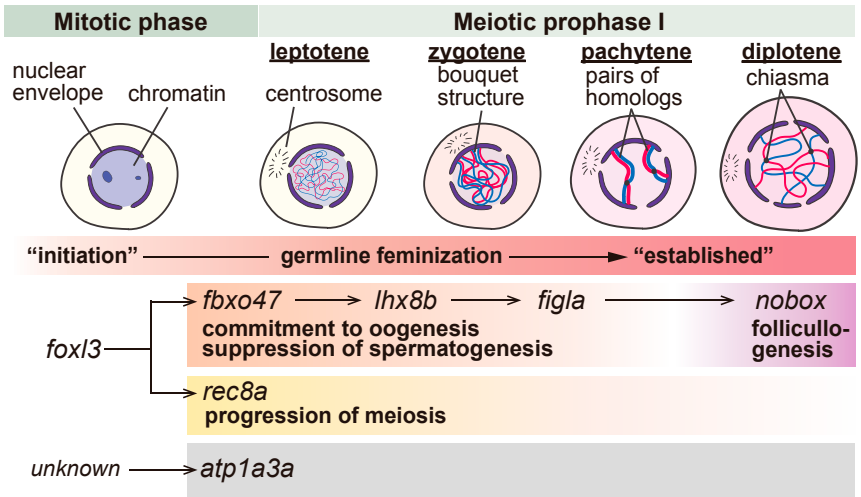


**Fig. 5.** Process of germline feminization in medaka. *foxl3*-dependent and *foxl3*-independent molecular pathways contribute to germline feminization. Downstream of *foxl3*, *fbxo47*, and *rec8a* promote folliculogenesis and meiosis, respectively. The *fbxo47*-downstream pathway, which is also important for oogenesis commitment, keeps germ cells in the oogenic pathway and prevents them from differentiating into spermatogenic cells. *atp1a3a* is up-regulated in female germ cells independently of *foxl3* (2).

## Materials and Methods

**Fish.** The OKcab strain of medaka fish (*O. latipes*) was used in this study. Fish were maintained in fresh water at 25–28 °C under a regulated photoperiod (14-h light and 10-h dark). All experiments were conducted with the approval of the Nagoya University official ethics committee (Approval no. 9 in the Department of Science, Nagoya University).

**Sex Genotyping.** Genotypic sex of all animals was determined by qPCR using TaqMan MGB probes (Thermo Fisher Scientific) that detect the male-determining gene *dmy* (32, 33) and the autosomal gene *cyp19a1* as a control (*SI Appendix*, Table S4). Genomic DNA was extracted from the larval head or tip of the caudal fin by freezing at −80 °C for 5 min and heating at 95 °C for 5 min. Extracted DNA was diluted and used as a PCR template. qPCR was performed using TaqMan Fast Advanced Master Mix on a StepOnePlus real-time PCR system (Thermo Fisher Scientific). Cycling parameters were as follows: 40 cycles of 95 °C for 3 s and 60 °C for 20 s. PCR primers used for genotyping are shown in *SI Appendix*, Table S4.

**Generation of KO Medaka Lines by CRISPR/Cas9.** CRISPR/Cas9 targeting sites were identified using the CRISPR/Cas9 target online predictor (CCTop; https://crispr.cos.uni-heidelberg.de/index.html). Selected target sites are shown in *SI Appendix*, Figs. S1, S5, S7, and S8.

To prepare template DNA for synthesis of guide RNAs (gRNAs) by in vitro transcription (IVT), we used two methods. For *lhx8b* and *nobox*, the designed oligonucleotides were annealed and cloned into vector DR274 (Addgene no. 42250) as described previously (16). For *rec8a* and *fbxo47*, we used a simplified method without cloning (34). Briefly, sense and antisense oligonucleotides were 5′-tagged with a T7 promoter and 15 bp of transactivating CRISPR (tracr) sequence, respectively. T7-promoter-target tracr was amplified by annealing and PCR with the following cycle parameters: 95 °C for 1 min; 32 cycles of 98 °C for 5 s; 55 °C for 15 s; and 68 °C for 1 min. PCR primer sets are shown in *SI Appendix*, Table S4. The resultant PCR products were used as templates for IVT. Protocols for gRNA synthesis, *Cas9* mRNA synthesis, and microinjection of gRNA and *Cas9* mRNA into medaka embryos were described previously (16). Each mutant allele was identified in the F1 generation by sequence analysis using the primer sets shown in *SI Appendix*, Table S4. KO efficiency of mutant lines is shown in *SI Appendix*, Table S5.

For analysis of the *fbxo47* function (Fig. 2), we established a method for inducing mutations efficiently in the germline of the F0 generation. *Cas9* fused with *nanos3 3′UTR* (*Cas9-nanos3 3′UTR*) mRNA was synthesized from vector pCS2+hSpCas9-nos3 3′UTR, which was generated by insertion of the *nanos3* 3′UTR sequence (35) into the *Xba*I site of vector pCS2+hSpCas9 (Addgene no. 51815). Efficiency of germline mutagenesis was evaluated by injecting gRNAs targeting DsRed and EGFP (*SI Appendix*, Table S4) into *olvas*-EGFP/*sox9b*-DeRed transgenic medaka (36, 37) (*SI Appendix*, Fig. S3). Two *fbxo47*-targeting gRNAs (*SI Appendix*, Table S4, 25 ng/μL each) and *Cas9-nanos3 3′UTR* mRNA (50 ng/μL) were coinjected into medaka embryos. Primers used for vector construction are shown in *SI Appendix*, Table S4.

To induce ectopic expression of *fbxo47* in *foxl3*$^{\Delta 17-/-}$ gonads (*SI Appendix*, Fig. S6), the *fbxo47* cassette (*fbxo47* ORF-*fbxo47* 3′UTR-BGHpA-*CAT*) and *olvasp*-EGFP cassette (*olvas* promoter-*EGFP* ORF-*olvas* 3′UTR-BGHpA-*Kmr*) were inserted into medaka BAC (clone name: ola1-212j01, purchased from NBRP Medaka [https://shigen.nig.ac.jp/medaka/]) by homologous recombination as previously described (38). *fbxo47* ORF-*fbxo47* 3′UTR was cloned into the *EGFP* locus of vector hsGBA-NCm by using an In-Fusion HD Cloning Kit (Takara no. 639648). hsGBA-NCm was generated by exchanging the *Kmr* gene of hsGBA-NKm (38) for the *CAT* gene of pACYC184 (Addgene no. 37033) by In-Fusion. The resultant vector was used as a PCR template to amplify the *fbxo47* cassette, which was recombined into the *foxl3* gene locus in the BAC (ola1-212j01) that contains the *olvasp*-EGFP cassette in the region between *foxl3* and *tmem201* (1). Primers used for vector construction and fragment amplification are listed in *SI Appendix*, Table S4. The resultant construct was injected into progeny of *foxl3*$^{\Delta 17+/-}$ females crossed with *foxl3*$^{\Delta 17-/-}$ males at the one-cell stage (1). Injected larvae were fixed at 10 dph and used for IHC. Injection and sampling data are summarized in *SI Appendix*, Table S3.

**In Situ Hybridization, IHC, and Histology.** Whole-mount in situ hybridization, immunohistochemistry, and PAS staining were performed as previously described (16, 39, 40). complementary DNA (cDNA) clones for *fbxo47* (NBRP clone name: olte61d07, RefSeq ID: XM_011489632) and *lhx8b* (NBRP clone name: olova4m02, RefSeq ID: XM_ 023965531) were purchased from NBRP Medaka. *rec8a* (RefSeq ID: XM_011485338) and *nobox* (RefSeq ID: XM_004074351) cDNAs were cloned from *meioC*$^{-/-}$ and wild-type ovarian cDNA libraries, respectively. Each cDNA was used as the PCR template for amplification of T7-promoter-tagged DNA, which was then used as an IVT template. PCR primers are shown in *SI Appendix*, Table S4. Digoxigenin-labeled RNA probes were synthesized as described previously (16).

Antiserum or antibodies for the following proteins were used in this study: medaka OLVAS (40) (1:100; rat), SYCP1 (41) (1:100; mouse), CC-3 (1:100, rabbit, CST no. 9661), FOXL3 (2) (1:200, mouse), and phosphorylated histone H3 (1:100, mouse, Millipore nos. 06–570). Secondary antibodies were Alexa Fluor 488-, 568-, and 647-conjugated goat antibodies (1:100, Thermo Fisher Scientific). IHC images were captured and analyzed on an Olympus FLUOVIEW FV1000.

**Preparation of Chromosomal Spreads.** Whole gonads were dissected and cut into 1-mm$^2$ fragments and treated with hypotonic solution (1% wt/vol trisodium citrate) for 15 min at room temperature. Tissues were placed on a slide glass, and fixative I (ethanol:acetic acid:$H_2O$ = 3:3:4) was dropped onto the tissues. When the fixative dried out, tissues were minced with fine forceps into pieces as small as possible. Residual fixative was removed, fixative I was added, and the sample was incubated at room temperature until the solution just started to dry. Fixative II (ethanol:acetic acid = 1:1) was added; just before the solution dried out, another fixative II was added. Finally, acetic acid was added, and the sample was dried completely. Slides were washed once with 50% methanol and stained with 4% Giemsa (Millipore no. 109204) in Sorenson's phosphate buffer (33.36-mM $KH_2PO_4$, 33.46-mM $Na_2HPO_4$, pH 6.8) for 15 min. Slides were washed with tap water, dried completely, and enclosed in Eukitt (ORSAtec).

Meiotic stages were determined in reference to the following chromosomal characteristics: At the zygotene stage, chromosomes are huddled together in a small compact mass. By the midpachytene stage, the size of the nucleus becomes larger, and all of the synapsed chromosomes are visible as fine threads within the nucleus. At the diplotene stage, each chromosome becomes distinguishable in the spermatocyte, while lampbrush chromosomes are formed in the oocyte. At metaphase I, one or two chiasmata between fully condensed homologs are observed, whereas such structures are not found at metaphase II. Secondary spermatocyte, round spermatid, and sperm can be distinguished on the basis of nuclear size.

In *SI Appendix*, Fig. S4, ovaries of adult *meioC*$^{-/-}$ XX were used as a control for normal mitotic chromosomes because they lack follicles (16), enabling us to obtain mitotic cells efficiently.

**Data Availability.** Data availability is described in the text and/or *SI Appendix* files.

**ACKNOWLEDGMENTS.** We thank Dr. Akira Kanamori of Nagoya University for providing the *figla* cDNA and Dr. Masakane Yamashita and Dr. Toshiharu Iwai of Hokkaido University for the SYCP1 antibody. We thank NBRP Medaka for the medaka cDNA clones and BAC. We are grateful to all members of the M.T. laboratory for helpful discussions and suggestions regarding the study. This work was supported by Research Fellowships of Japan Society for the Promotion of Science for Young Scientists (Grant 16J16351: M.K.), a Grant-in-Aid for Young Scientists (B) (16K18557: T.N.), a Grant-in-Aid for Scientific Research on Innovative Areas (17H06430: M.T.), a Grant-in-Aid for Scientific Research (A) (16H02514: M.T.), and the National Agriculture and Food Research Organization Bio-oriented Technology Research Advancement Institution (Research Program on Development of Innovative Technology, 29007A: M.T.).

1. T. Nishimura *et al.*, Sex determination. foxl3 is a germ cell-intrinsic factor involved in sperm-egg fate decision in medaka. *Science* **349**, 328–331 (2015).
2. M. Kikuchi *et al.*, Novel components of germline sex determination acting downstream of foxl3 in medaka. *Dev. Biol.* **445**, 80–89 (2019).
3. I. Braasch *et al.*, The spotted gar genome illuminates vertebrate evolution and facilitates human-teleost comparisons. *Nat. Genet.* **48**, 427–437 (2016).
4. K. I. Ishiguro, The cohesin complex in mammalian meiosis. *Genes Cells* **24**, 6–30 (2019).
5. L. A. Bannister, L. G. Reinholdt, R. J. Munroe, J. C. Schimenti, Positional cloning and characterization of mouse mei8, a disrupted allelle of the meiotic cohesin Rec8. *Genesis* **40**, 184–194 (2004).
6. H. Xu, M. D. Beasley, W. D. Warren, G. T. van der Horst, M. J. McKay, Absence of mouse REC8 cohesin promotes synapsis of sister chromatids in meiosis. *Dev. Cell* **8**, 949–961 (2005).
7. T. Cardozo, M. Pagano, The SCF ubiquitin ligase: Insights into a molecular machine. *Nat. Rev. Mol. Cell Biol.* **5**, 739–751 (2004).

8. Y. Chen *et al*., Single-cell RNA-seq uncovers dynamic processes and critical regulators in mouse spermatogenesis. *Cell Res.* **28**, 879–896 (2018).
9. V. Jantsch *et al*., Caenorhabditis elegans prom-1 is required for meiotic prophase progression and homologous chromosome pairing. *Mol. Biol. Cell* **18**, 4911–4920 (2007).
10. A. Mohammad *et al*., Initiation of meiotic development is controlled by three post-transcriptional pathways in Caenorhabditis elegans. *Genetics* **209**, 1197–1224 (2018).
11. S. A. Pangas *et al*., Oogenesis requires germ cell-specific transcriptional regulators Sohlh1 and Lhx8. *Proc. Natl. Acad. Sci. U.S.A.* **103**, 8090–8095 (2006).
12. Y. Choi, D. J. Ballow, Y. Xin, A. Rajkovic, Lim homeobox gene, lhx8, is essential for mouse oocyte differentiation and survival. *Biol. Reprod.* **79**, 442–449 (2008).
13. L. Liang, S. M. Soyal, J. Dean, FIGalpha, a germ cell specific transcription factor involved in the coordinate expression of the zona pellucida genes. *Development* **124**, 4939–4947 (1997).
14. S. M. Soyal, A. Amleh, J. Dean, FIGalpha, a germ cell-specific transcription factor required for ovarian follicle formation. *Development* **127**, 4645–4654 (2000).
15. A. Rajkovic, S. A. Pangas, D. Ballow, N. Suzumori, M. M. Matzuk, NOBOX deficiency disrupts early folliculogenesis and oocyte-specific gene expression. *Science* **305**, 1157–1159 (2004).
16. T. Nishimura *et al*., Germ cells in the teleost fish medaka have an inherent feminizing effect. *PLoS Genet.* **14**, e1007259 (2018).
17. Q. Wu *et al*., Sexual fate change of XX germ cells caused by the deletion of SMAD4 and STRA8 independent of somatic sex reprogramming. *PLoS Biol.* **14**, e1002553 (2016).
18. S. I. Nagaoka *et al*., ZGLP1 is a determinant for the oogenic fate in mice. *Science* **367**, eaaw4115 (2020).
19. J. Bowles *et al*., Retinoid signaling determines germ cell fate in mice. *Science* **312**, 596–600 (2006).
20. J. Koubova *et al*., Retinoic acid regulates sex-specific timing of meiotic initiation in mice. *Proc. Natl. Acad. Sci. U.S.A.* **103**, 2474–2479 (2006).
21. K. -I. Ishiguro *et al*., MEIOSIN directs the switch from mitosis to meiosis in mammalian germ cells. *Dev. Cell* **52**, 429–445.e10 (2020).
22. G. A. Dokshin, A. E. Baltus, J. J. Eppig, D. C. Page, Oocyte differentiation is genetically dissociable from meiosis in mice. *Nat. Genet.* **45**, 877–883 (2013).
23. M. C. Adolfi *et al*., Retinoic acid and meiosis induction in adult versus embryonic gonads of medaka. *Sci. Rep.* **6**, 34281 (2016).
24. J. Pasquier *et al*., Gene evolution and gene expression after whole genome duplication in fish: The PhyloFish database. *BMC Genomics* **17**, 368 (2016).
25. C. K. Cahoon, D. E. Libuda, Leagues of their own: Sexually dimorphic features of meiotic prophase I. *Chromosoma* **128**, 199–214 (2019).
26. C. Tease, M. A. Hultén, Inter-sex variation in synaptonemal complex lengths largely determine the different recombination rates in male and female germ cells. *Cytogenet. Genome Res.* **107**, 208–215 (2004).
27. K. Brick *et al*., Extensive sex differences at the initiation of genetic recombination. *Nature* **561**, 338–342 (2018).
28. J. M. Sardell *et al*., Sex differences in recombination in sticklebacks. *G3 (Bethesda)* **8**, 1971–1983 (2018).
29. S. Wang *et al*., Per-nucleus crossover covariation and implications for evolution. *Cell* **177**, 326–338.e16 (2019).
30. Y. He *et al*., MEIOTIC F-BOX is essential for male meiotic DNA double-strand break repair in rice. *Plant Cell* **28**, 1879–1893 (2016).
31. F. Zhang *et al*., The F-box protein ZYGO1 mediates bouquet formation to promote homologous pairing, synapsis, and recombination in rice meiosis. *Plant Cell* **29**, 2597–2609 (2017).
32. M. Matsuda *et al*., DMY is a Y-specific DM-domain gene required for male development in the medaka fish. *Nature* **417**, 559–563 (2002).
33. I. Nanda *et al*., A duplicated copy of DMRT1 in the sex-determining region of the Y chromosome of the medaka, Oryzias latipes. *Proc. Natl. Acad. Sci. U.S.A.* **99**, 11778–11783 (2002).
34. X. Liang *et al*., Rapid and highly efficient mammalian cell engineering via Cas9 protein transfection. *J. Biotechnol.* **208**, 44–53 (2015).
35. H. Kurokawa *et al*., Time-lapse analysis reveals different modes of primordial germ cell migration in the medaka Oryzias latipes. *Dev. Growth Differ.* **48**, 209–221 (2006).
36. M. Tanaka, M. Kinoshita, D. Kobayashi, Y. Nagahama, Establishment of medaka (Oryzias latipes) transgenic lines with the expression of green fluorescent protein fluorescence exclusively in germ cells: A useful model to monitor germ cells in a live vertebrate. *Proc. Natl. Acad. Sci. U.S.A.* **98**, 2544–2549 (2001).
37. S. Nakamura, K. Kobayashi, T. Nishimura, S. Higashijima, M. Tanaka, Identification of germline stem cells in the ovary of the teleost medaka. *Science* **328**, 1561–1563 (2010).
38. S. Nakamura, D. Saito, M. Tanaka, Generation of transgenic medaka using modified bacterial artificial chromosome. *Dev. Growth Differ.* **50**, 415–419 (2008).
39. S. Nakamura *et al*., Identification and lineage tracing of two populations of somatic gonadal precursors in medaka embryos. *Dev. Biol.* **295**, 678–688 (2006).
40. Y. Aoki *et al*., Temporal and spatial localization of three germline-specific proteins in medaka. *Dev. Dyn.* **237**, 800–807 (2008).
41. T. Iwai *et al*., Structural components of the synaptonemal complex, SYCP1 and SYCP3, in the medaka fish Oryzias latipes. *Exp. Cell Res.* **312**, 2528–2537 (2006).